

A heterarchical multiscale model for granular materials with evolving grainsize distribution

Benjy Marks¹  · Itai Einav¹

Received: 20 December 2016 / Published online: 24 July 2017
© Springer-Verlag GmbH Germany 2017

Abstract Naturally occurring granular flows, such as landslides, debris flows and avalanches typically have size ratios of up to 10^6 between the smallest and largest constituent particles. For the purposes of modelling, however, it is generally assumed that a single representative size can adequately describe the grains. Polydisperse flows are not described more completely primarily because of two reasons: The first is a lack of understanding of the physical mechanisms which affect polydisperse flows. The second is a lack of models with which to describe such systems. Here, we present a heterarchical multiscale model which accounts for both the microstructural evolution within representative elementary volumes, and also the associated changes in bulk flow properties. Three key mechanisms are addressed; segregation, comminution and mixing. Granular segregation is an important mechanism for industrial processes aiming at mixing grains. Additionally, it plays a pivotal role in determining the kinematics of geophysical flows. Because of segregation, the grainsize distribution in a granular medium varies in space and time during flow. Additional complications arise from the presence of comminution, where new particles are created, potentially enhancing segregation. This has a feedback on the comminution process, as particles change their local neighbourhood. Simultaneously, particles are generally undergoing remixing, further complicating the segregation and comminution processes. The interaction between these mechanisms is explored using a stochastic lattice model with three rules: one for each of segregation, comminution and mixing. The interplay between these rules creates complex patterns, as seen in segregating systems, and depth depen-

dent log-normal grading curves, which have been observed in avalanche runout.

Keywords Multiscale modelling · Segregation · Comminution · Mixing · Granular flows

1 Introduction

The dynamics of flowing granular material are important in many natural processes, such as debris flows, landslides, rockfalls and shear banding. Industrial processing also requires many granular flows, such as rotating or tumbling mills, chute flows and hopper filling or discharge. It is often postulated that these flows can be described in terms of conventional continuum mechanics, with an appropriate constitutive model that represents the bulk behaviour [1]. At the same time, it is also well understood that these same flows typically exhibit complex behaviour, including many phenomena that cannot be described in the context of a conventional continuum. For example, size segregation [2,3], agglomeration [4,5] and comminution in closed systems [6] all have no analogue in continuum mechanics. One method to include these phenomena in open systems is to involve the grainsize distribution as a dynamic property of the continuum [7].

The description of granular material can in general be divided into two fields, being either a statistical ensemble of a set of discrete particles, or a continuum [8]. If we wish to describe a granular flow as a continuum, while still retaining the relevant micromechanical behaviour, the accepted methodology is via upscaling, or coarse-graining [9,10]. Using these methods, we vastly decrease the amount of information at the representative volume element (RVE) level, from the positions, velocities and forces acting on every par-

✉ Benjy Marks
benjy.marks@sydney.edu.au

¹ Particles and Grains Laboratory, The University of Sydney, Sydney 2006, Australia

ticle, to a small set of continuum properties which represent the bulk behaviour. One key element which is lost in such a process is the local arrangement of each particle, and its' corresponding loading state. For the case of comminution, the breakage mechanics theory has been applied successfully to describe how grainsize distribution evolves and affects the constitutive response of brittle granular material in closed systems [6], and it is well understood that both the typical fracture energy and the fragment size distribution are functions of the loading state of the individual particle [11, 12]. Currently, there are no spatio-temporal continuum models for measuring changes in the grainsize distribution for such open systems where particles can both advect in space and simultaneously change in size.

As shown in Fig. 1, typical multiscale models are *hierarchical*, coupling distinctly different models at different length scales. Take for example coupled FEM–DEM models [13, 14], which replace a constitutive model in a finite element simulation with a discrete element simulation at each gauss point. Here, we propose a new paradigm for constructing multiscale models—a *heterarchical* model. This model, in contrast to a hierarchical one, loses the strict distinction between the two scales, allowing information to be passed not only from scale to scale, but from the microscale within one RVE to another RVE.

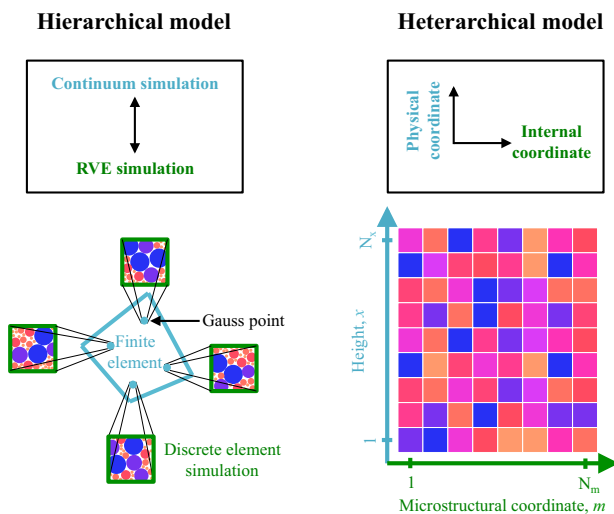


Fig. 1 Alternative structures for multiscale models. *Top left* a hierarchical model, where information is passed between two distinct simulations, each at different length scales. *Top right* a heterarchical model, where the two length scales are coupled directly as orthogonal directions in a single model. *Bottom left* a typical example of a hierarchical model, where a constitutive model in a finite element simulation is replaced with a separate discrete element simulation. *Bottom right* The heterarchical model presented here, where the two scales coexist in the same framework. In all cases, *light blue* represents the continuum scale, and *green* represents the representative volume element scale (colour figure online)

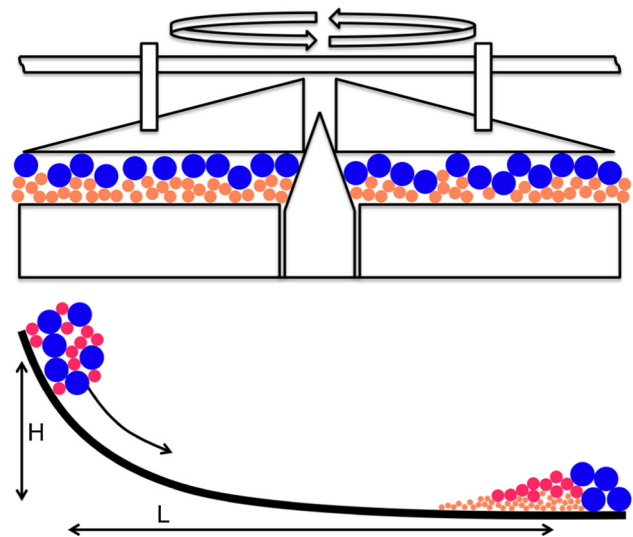


Fig. 2 *Top* a mill stone—the grinding of wheat grain using a mill stone is one of the oldest industrial problems in human history, yet still mathematically unsolved. Particles of wheat grain are crushed to a fine powder by very large deformation shearing at high normal stress. The fine powder segregates out of the shear zone into cavities built into the mill stone, and then under the action of centripetal forces migrates out to a collection bin. *Bottom* a long run-out landslide, where the ratio of L/H can be up to 10. L and H are the change in horizontal position and height respectively of the centre of mass of an avalanche during run-out. Large values of L/H are possible indicators of lubrication by a layer of very small particles at the base of the flow, which have been created as a result of comminution and percolated downwards through segregation

These effects are especially important in two poorly understood systems, shown in Fig. 2. The first is ancient grain milling, where combined normal and shear stresses crush wheat grains, dynamically sieving the resultant mix. The second is long run out avalanches, where it is unclear why these incredibly destructive natural phenomena can travel enormous distances, up to 10 times their vertical fall [15, 16]. With regards to debris flows, it has been understood for some time that there is a need to model spatial and temporal variability in the grainsize distribution of flowing material to be able to implement appropriate rheological models [17].

2 A grainsize enriched continuum

A convenient formulation to describe a polydisperse material as a continuum is that of population balance equations [7, 18, 19]. In addition to the usual properties of a continuum, which are described as functions of physical space and time coordinates, the population balance framework allows for the inclusion of *internal coordinates*. Here we define two choices of internal coordinate which can be used to describe the microscale of a polydisperse material. Either the internal coordinate can represent the physical size of the constituent particles, which we denote the *grainsize* coordinate s , as in

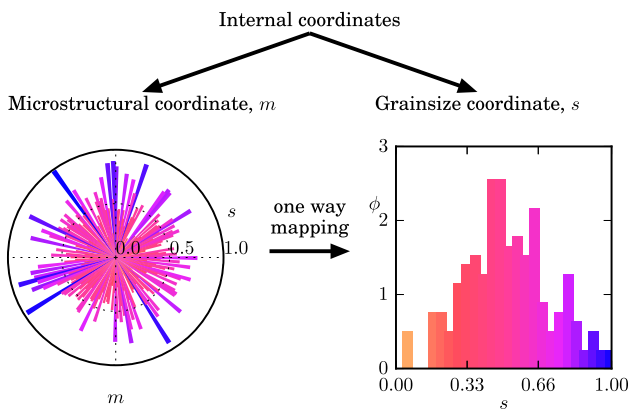


Fig. 3 Two representations of information internal to a representative volume element. *Left* the arrangement of grain size s along the microstructural coordinate m . This coordinate is assumed here to be cyclic, and so is shown on a polar plot. *Right* the grainsize distribution is a normalised histogram of the grain sizes along a grainsize coordinate s . Information can only be passed in one direction from the microstructural coordinate to the grainsize coordinate

[7], or the coordinate(s) can be a discretisation of the volume within the RVE, such that distance along the coordinate axis/axes represents somehow the local neighbourhood of particles, which we will name as the *microstructural* coordinate(s). A comparison of each of these assumptions for a single RVE is shown in Fig. 3.

For the case of a grainsize coordinate s , as in [7], the internal coordinate allows for every point in space to have a grainsize distribution which can evolve with time. We then describe this continuous grainsize distribution $\phi(s)$ of the system in terms of the solid fraction $\Phi(s)$ of particles between grainsizes s_a and s_b as

$$\Phi[s_a < s < s_b] = \int_{s_a}^{s_b} \phi(s') ds'. \tag{1}$$

Following [7, 18, 19], conservation of mass at a point in space $\mathbf{r} = \{x, y, z\}$ can then be expressed as

$$\frac{\partial \phi}{\partial t} + \nabla \cdot (\phi \mathbf{u}) = h^+ - h^-, \tag{2}$$

where $\mathbf{u}(\mathbf{r}, s, t) = \{u, v, w\}$ is the material velocity, $h^+(\mathbf{r}, s, t)$ is the birth rate, describing the creation of new particles of grainsize s at time t , and $h^-(\mathbf{r}, s, t)$ is the death rate, at which particles of grainsize s are destroyed.

The second term in Eq. 2 describes the advection of mass, such as characterises open systems, where material can move in physical space. The right hand side of the same Equation represents mechanisms traditionally treated exclusively in closed systems, such as agglomeration, crushing and abrasion. Each of these systems — open and closed—has been the subject of much study, but the coupling of such processes using a continuum description has yet to be achieved.

3 Discretising heterarchical multiscale continua

In the interest of constructing a heterarchical multiscale model, we then wish to describe both the continuum-level properties, and those at the scale of the REV itself, in one rational framework. For this purpose, we turn to the stochastic lattice model defined in [20]. This model consists of a regular cartesian lattice in $D + S$ dimensions, where D is the number of *external* or *physical* coordinates, and S is the number of *microstructural* coordinates. We treat the external and microstructural coordinates as a higher dimensional continuum, such that each coordinate is orthogonal to the others.

For the following, a single spatial/physical coordinate, x , and a single microstructural coordinate, m , are considered, although generalisation to higher dimensions is straightforward. The system is then discretised into a regular cartesian grid, numbered from the bottom-left corner, so that position on the grid can be expressed using the pair $\{x_i, m_j\}$, where i and j indicate the number of cells across in the respective x and m directions, as shown in Fig. 1, with X and M the total number of cells in each direction. In all cases the system is considered to be cyclic in the m direction, such that $j \equiv j \bmod M$, where $\bmod M$ is the modulo operator. Each cell contains a single number, $s_{i,j}$, which dictates the grainsize of the particles in the RVE defined by the row i , as shown in Fig. 3. Furthermore, we consider the local neighbourhood of a particular particle as those that are adjacent in the m direction. The m direction now contains more information than the grainsize distribution alone, as the local configuration of particles is preserved, below the resolution of the analogous continuum scale.

We can now connect the microstructural coordinate m to the grainsize coordinate s (as illustrated in Fig. 3). This is done by defining a discretised grainsize distribution ϕ_i at any height x_i as a histogram of the number of cells within a discrete grainsize fraction with centre s_a and width Δs in all M neighbours taken in the m direction as

$$\phi_i(s_a) = \frac{1}{M \Delta s} \sum_{j=1}^M \mathcal{H} \left(\frac{\Delta s}{2} - |s_{i,j} - s_a| \right), \tag{3}$$

where \mathcal{H} is the Heaviside step function. We also define the local average grainsize over the nearest two neighbours in the m -direction as

$$\bar{s}_{i,j} = \frac{s_{i,j-1} + s_{i,j+1}}{2}, \tag{4}$$

although any number of nearest neighbours can in general be used to define the local neighbourhood size. A more general average grainsize could be defined nonlocally along the microstructural coordinate (e.g., considering a vector of

left and right neighbours $s_{i,j-n}$ and $s_{i,j+n}$ with appropriate weights). Another possibility is to increase the number of microstructure coordinates with a variety of possible stencils. However, for the sake of simplicity these possibilities are not explored in this paper.

We will next construct an equivalent continuum model, based on population balance equations, so that in the limit of infinitesimal cell size we can show that the stochastic lattice may be regarded as a first order partial differential solver [21]. In fact, there are many ways to recover continuous results from such a system [22].

4 Closed systems

We begin by considering closed systems, which are those in which material does not advect in space, such that $\mathbf{u} = \mathbf{0}$. There are many processes that have previously been represented as closed systems, such as comminution, agglomeration and abrasion. We here describe only comminution, where particles are crushed to form fragments of smaller sizes.

Following the formulation in [19], for the case where particles are created only by the fragmentation of larger particles, we can express the death rate as

$$h^-(s, t) = b(s)\phi(s, t), \tag{5}$$

where $b(s)$ is some specific breakage rate which governs the frequency at which particles of grainsize s break into smaller fragments. The birth rate is then the sum of breakages into size s over all particles larger than s , which can be expressed as

$$h^+(s, t) = \int_s^\infty b(s')P(s|s')\phi(s', t) ds', \tag{6}$$

where $P(s|s')$ is a probability density function which dictates the probability of creating grainsize s from crushing a particle of grainsize s' . Using (2), we can then express conservation of mass as

$$\frac{\partial \phi(s, t)}{\partial t} = \int_s^\infty b(s')P(s|s')\phi(s', t) ds' - b(s)\phi(s, t). \tag{7}$$

In a discrete sense, such as that defined in the stochastic lattice, we can rewrite this equation as the conservation of a grainsize fraction with centre s_a and width Δs , over a time step Δt as

$$\frac{\Delta \phi_i(s_a)}{\Delta t} = \sum_{k=a+\Delta s}^{N_s} \left(b_i(s_k)P(s_a|s_k)\phi_i(s_k)\Delta s \right) - b_i(s_a)\phi_i(s_a), \tag{8}$$

where N_s is the total number of evenly spaced bins of size Δs . These equations have been extensively investigated [23–26] and solutions have been proposed for many mechanisms of comminution, such as grinding, cleavage and abrasion. However, breakage mechanisms are normally assumed with a priori knowledge that the grainsize distribution will evolve towards a power law [18,23]. In fact, in most models, either the breakage rate b , the fragment size distribution P , or both, are generally assumed to be power law in nature from the outset [23]. For high velocity impacts, power law fragment size distributions are often measured due to single impact events [27]. At the low relative velocities and higher coordination numbers experienced in a granular flow, however, the fragment size distribution appears to follow a Weibull distribution [28,29].

Another method to model the problem has been proposed in various forms, and uses simple geometric analogies in a cellular automaton [30,31] where power law patterns are found, not imposed, by assuming that particles with neighbours of the same size are likely candidates to crush. We can unify these two approaches, of macroscopic grainsize distribution changes, and microscopic nearest neighbourhood behaviour, by including a microstructural coordinate in a stochastic lattice model.

4.1 Comminution

The process of comminution has two complimentary components which we must define. Firstly, there is a particular loading state at which individual particles will crush. Secondly, there is a fragment size distribution which defines the products that are created when the particle crushes. We can define a crushing event as:

$$\text{if } \sigma_{i,j}^t \geq \sigma_{i,j}^c : \quad s_{i,j}(t + \Delta t) = Xs_{i,j}(t), \tag{9}$$

where $\sigma_{i,j}^t$ is the maximal tensile stress within a given particle, and $\sigma_{i,j}^c$ is the maximal tensile stress at which the particle crushes, and X is an independent random variable pulled from an appropriate fragment size distribution. We can then measure a coarse grained breakage rate as the fraction of particles broken in a given time increment, as

$$b_i(s_a) = \frac{\sum_{j=1}^M \mathcal{H}(\sigma_{i,j}^t - \sigma_{i,j}^c) \mathcal{H}(\frac{\Delta s}{2} - |s_{i,j} - s_a|)}{M\phi_i(s_a)\Delta t}. \tag{10}$$

In [20], a crushing rule was proposed for a stochastic lattice model. This was a purely phenomenological model, which eschewed the idea of stress. Here, a more complete model is derived, beginning with the assumption of a Weibull distribution of flaws within each particle, such that the probability

of a particle of the maximum size surviving at a given stress is given by

$$P_{survival} = e^{-(\sigma^c/\sigma_M^c)^m} \tag{11}$$

Following [31,32], this is used to define the tensile stress at which a particle of given size is likely to crush, subject to diametric loading, which gives

$$\sigma_{i,j}^c(s) = \sigma_M^c \left(\frac{s_{i,j}}{s_M} \right)^{-3/w} \tag{12}$$

where the largest particle, with size s_M , will crush at σ_M^c , independent of the Weibull parameter w . A large value of w indicates that the material is quite uniform, and that a set of particles of a given size is likely to break within a small range of stresses. To measure σ_M^c and w , one could crush a set of particles of similar size, measure their fragmentation stress, and fitting (11). We define a mapping ζ which relates the maximum tensile stress within each particle, $\sigma_{i,j}^t$, to the bulk applied stress, σ^b , such that $\sigma_{i,j}^t = \zeta_{i,j} \sigma^b$. The mapping between these two stress fields can be related to the coordination number $Z_{i,j}$, which we define as

$$Z_{i,j} = Z_0 \left(\frac{s_{i,j}}{\bar{s}_{i,j}} \right)^2 \tag{13}$$

where Z_0 is the expectation value of the coordination number of a particle of the average size, and the coordination number is assumed to scale with the particle surface area, as measured in [33]. Three cases are shown schematically at the top of Fig. 4. If a given particle has very few contacts, it is unlikely to experience significant tensile stress, due to a lack of confinement. Conversely, if a particle has many contacts, it is in an isotropic compression loading state, and will also have a low internal tensile stress. The middle case, which describes particles with a moderate number of contacts, for simplicity taken here to be equal to Z_0 , will experience relatively large internal tensile stress. We therefore define a function ζ that scales with the coordination number, and is unity at $s = \bar{s}$. One promising example is the lognormal distribution,

$$\zeta_{i,j} = e^{-\frac{\log(s_{i,j}/\bar{s}_{i,j})^2}{2n^2}} \tag{14}$$

for which examples are shown in the bottom of Fig. 4 for three values of the scaling parameter n . We now have all the ingredients we need to define a crushing event. Crushing will occur if the applied tensile stress is greater than or equal to the crushing tensile stress, i.e. $\sigma_{i,j}^t \geq \sigma_{i,j}^c$ then,

$$\sigma^* \geq \left(\frac{s_{i,j}}{s_M} \right)^{-3/w} e^{\frac{\log(s_{i,j}/\bar{s}_{i,j})^2}{2n^2}} \tag{15}$$

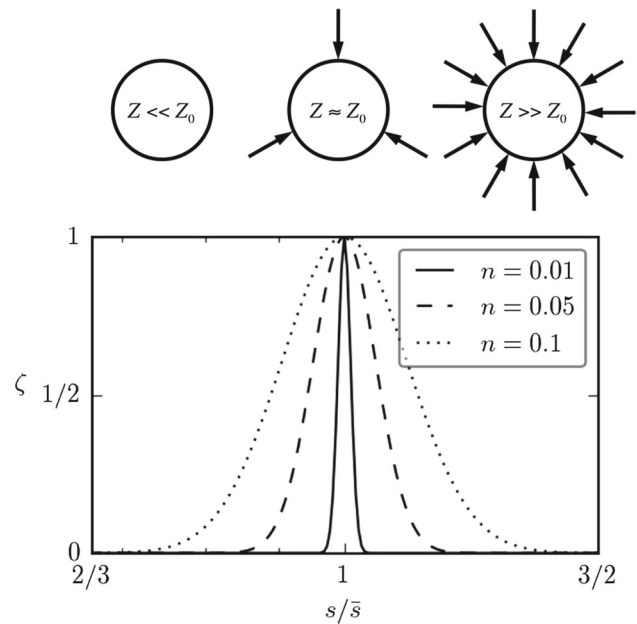


Fig. 4 The cushioning effect. *Top* an idealisation of loading conditions on a single particle as a function of coordination number, Z . *Bottom* the stress mapping function ζ , relating the macroscopic confining stress to the maximum internal tensile stress in a particle. Note that the abscissa is log-scaled

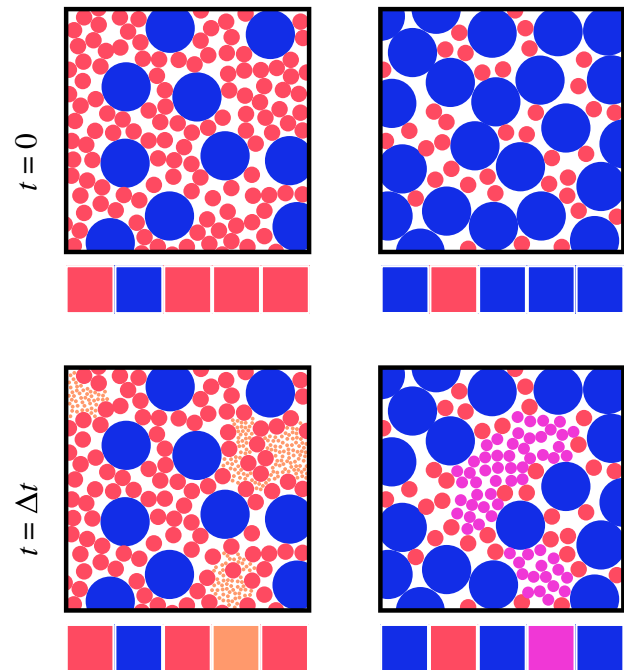


Fig. 5 The cushioning effect and nearest neighbour rule. *Left* large particles are cushioned such that they will not break because of an abundance of small particles. *Right* small particles do not carry a significant amount of load as they are free to move in the interstitial pore spaces. *Top* initial conditions. *Bottom* result after one iteration of the stochastic lattice rule, where on the left the small particles in a cell (red) become even smaller (orange), and on the right the large particles in a cell (blue) become smaller (pink) (colour figure online)

where we have defined the normalised loading state as $\sigma^* = \sigma^b / \sigma_M^c$. A schematic example of two cases of crushing is shown in Fig. 5, where the grainsize in cells which pass this criteria is reduced. To predict the updated grainsize in the cells, we need to define a fragment size distribution, $P(s|s')$, which is the probability of creating a particle of size s given the crushing of a particle of size s' . In general, it is believed that the fragment size distribution should not control significantly the behaviour of the system [32]. At the same time, the most commonly used fragment size distributions are either based on power laws, or Weibull distributions [28, 29, 34, 35]. Both of these distributions are heavy-tailed, and have power law dependence for small fragments, such that we will always create new fragments which follow a prescribed grading. To test the behaviour of the system, two alternative fragment size distributions are investigated (Weibull and Dirac delta function):

1. $P(s|s') = \frac{\frac{k}{\lambda} \left(\frac{s}{\lambda s'}\right)^{k-1} e^{-\left(\frac{s}{\lambda s'}\right)^k}}{1 - e^{-\lambda^{-k}}}$,
2. $P(s|s') = \delta(s - cs')$, the size is reduced by a constant value c ,

and where k and λ are in general material and size dependent parameters. Examples of the behaviour of these rules are

shown in Figs. 6 and 7 for a range of initial conditions and system parameters. In each case, the simulation is run for X cells, spaced Δs apart. Initial conditions are generated by sampling X times from $F = \Delta s$ to $F = 1$ linearly along the inverse power law distributions defined by

$$s = F^{1/(3-\alpha_i)} \tag{16}$$

where $F(s) = \int_{s_m}^s \phi(s') ds'$ is the cumulative grainsize distribution function and $3 - \alpha_i$ is the initial power law gradient. The simulation progresses by slowly raising the normalised applied stress, σ^* , from an initial value of 0 to its maximum value.

For the case of constant size reduction, Fig. 6 shows separately the effect of varying σ^* , n , w and c . Increasing σ^* increases the applied load, creating progressively smaller fragments. The collective behaviour progresses towards a power-law grainsize distribution, with slope $\alpha = 1.99$. The width of the stress mapping ζ is controlled by n , which affects the slope of the produced power law grainsize distribution. The strength parameter w controls the shape of the tail of the produced grainsize distribution, but does not affect the power-law component. The size reduction ratio, c , creates strong discontinuities in the grainsize distribution if small,

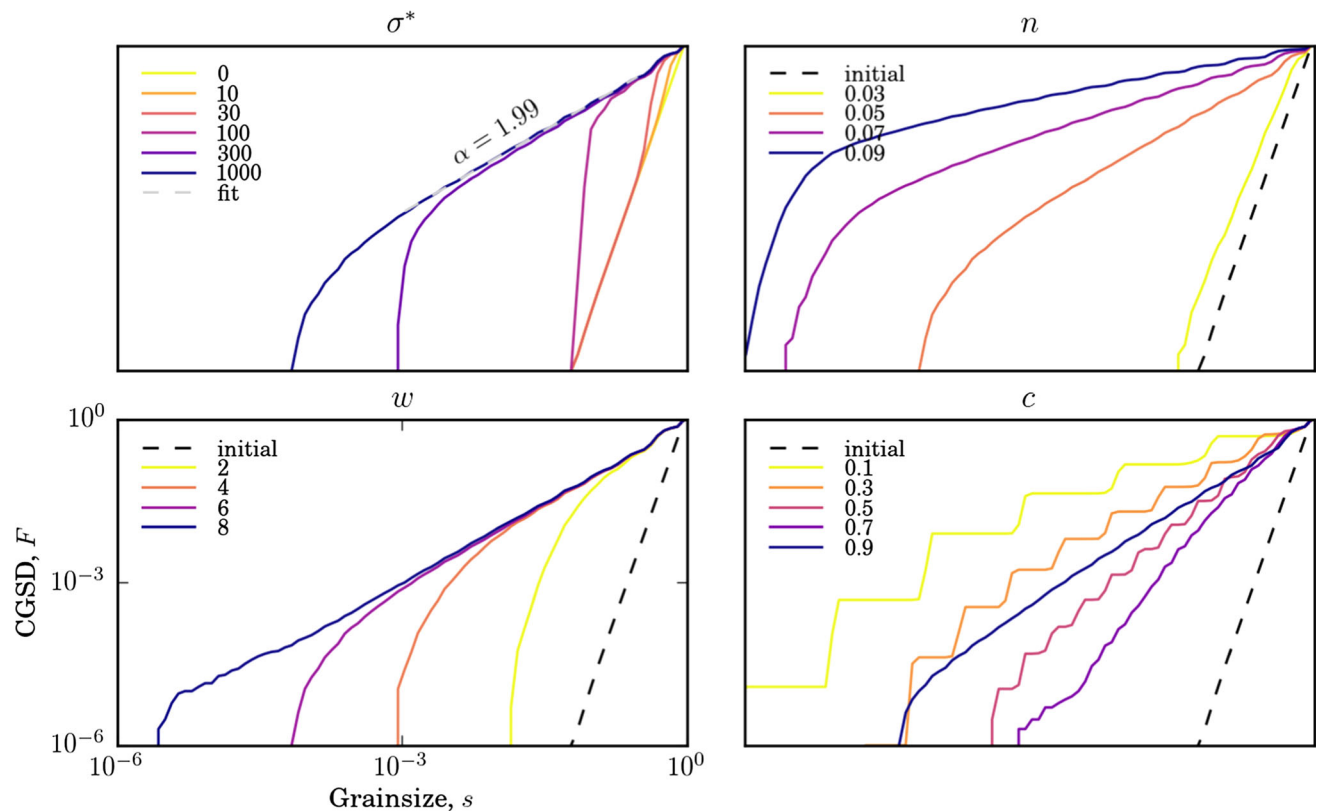


Fig. 6 Evolution of the system for various system configurations using a constant fragment size distribution $P(s|s') = \delta(s - cs')$. For all cases $M = 10^6$ and σ^* is increased from 0 to 10^3 . The slope of power law part

of the curve is $3 - \alpha$. Unless otherwise indicated, $n = 0.05$, $c = 0.8$ and $w = 6$. The title of each *subfigure* indicates the property being varied

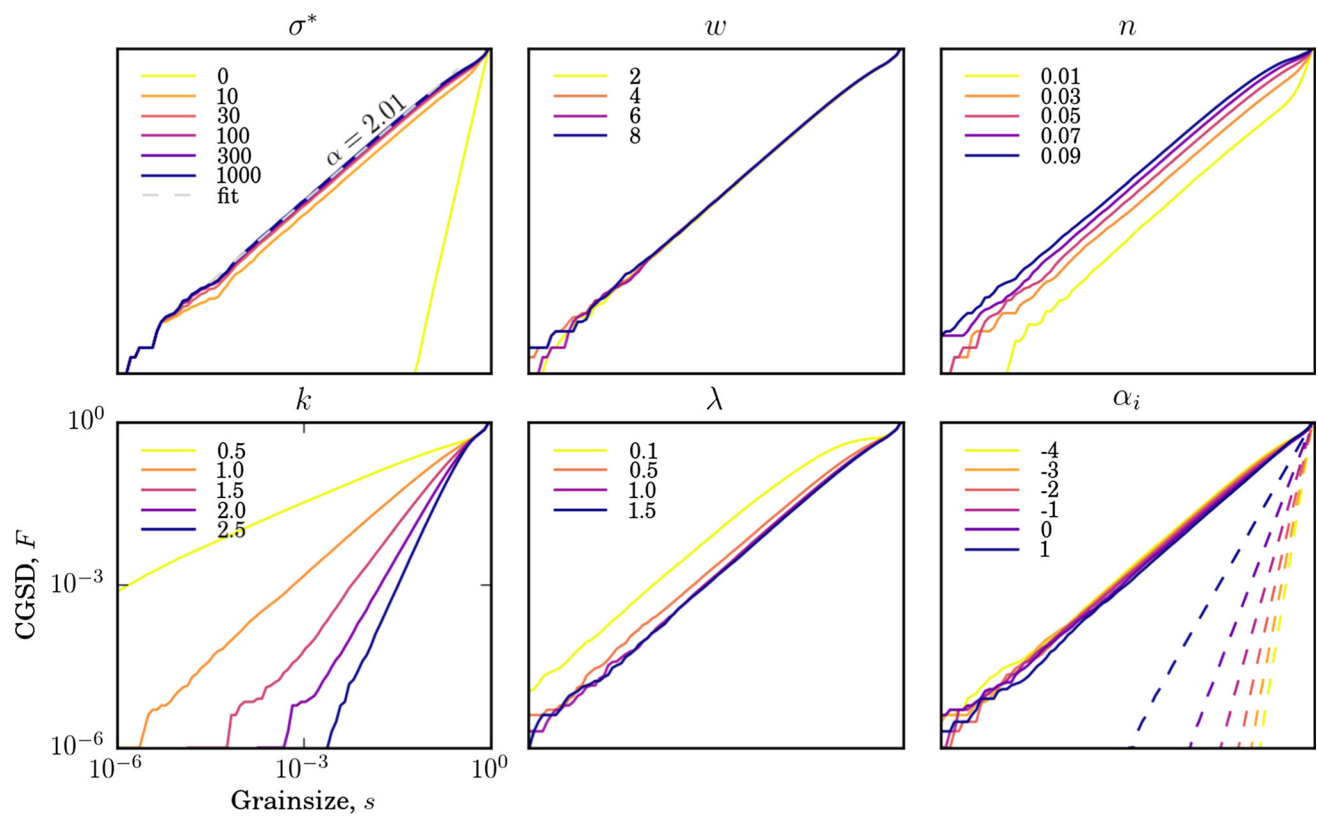


Fig. 7 Evolution of the system for various system configurations using a Weibull fragment size distribution. For all cases $M = 10^6$ and σ^* is slowly increased from 0 to 10^3 . Unless otherwise indicated, $w = 3$,

$n = 0.05$, $k = 1$, $\lambda = 1$ and $\alpha_i = -2$. The title of each *subfigure* indicates the property being varied

however globally a power-law grainsize distribution is still measurable. As the value of c increases, the grainsize distribution becomes smoother. In all cases, the final grainsize distribution does not significantly depend on the initial grading, α_i , as previously concluded through discrete element simulations [32].

Figure 7 shows a similar evolution towards a power-law grainsize distribution, but using a Weibull fragment size distribution. During loading, the smallest fragments are created with a power law grading, dictated by the fragment size distribution, and significant further crushing does not occur. The slope of the power law is insensitive to changes of w , n , λ and α_i .

Given that we measure Weibull-distributed fragment sizes experimentally, it is then instructive to ask: Which of the two proposed fragment size distributions is more effective at modelling real systems? The Weibull distribution assumes that arbitrarily small particles can be created as a result of comminution. This prediction, together with the requirement for an additional fitting parameter, leads us to prefer the rule of constant size reduction.

For both fragment size distributions, the stochastic lattice model predicts the same final grainsize distribution largely independent of the initial grading. Such a power law grading

of the grainsize distribution has been measured in cellular automata [30,31], discrete element simulations [36] and experiment [16].

Generally fractal dimensions are measured in fault gauges, confined comminution tests and rock avalanches in the range of $\alpha = 2 - 3$ [27,37,38]. The limiting value of $\alpha = 2$ for most cases of our model can be explained using the cellular automaton developed in [27], where every particle in the systems has the same probability of crushing, given some additional geometric constraints. If this probability is exactly 0.5, the system develops a fractal dimension of $\alpha = 2$. If the probability is 1, the system reaches $\alpha = 3$, which represents a system with large strain, where nearest neighbours change over the crushing period [39]. A distribution with intermediate fractal dimension of around 2.5 corresponds to a random appollonian packing, as in [40].

In Fig. 8, α is measured many times from different regions of a single simulation. A number of cells, L , centred at a , are chosen, and a best fit of α is measured for the cumulative grainsize distribution. For values of $L > 10^5$, the measured power law does not change slope significantly. This is an indication of a fractal distribution [30].

The idea of such final power law grainsize distributions has been applied in [6] to develop a thermodynamically consis-

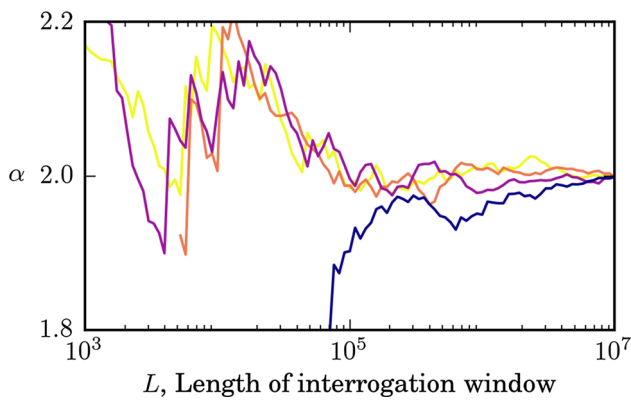


Fig. 8 Fractal dimension α measured as a function of interrogation window length L . The value of α is measured as a best fit of the cumulative grainsize distribution from $s = 10^{-3}$ to 10^{-1} , restricted to the cells between $j = a \pm L/2$. Each line represents a different value of $a = 0, N_x/4, N_x/2$ and $3N_x/4$. For this simulation $N_x = 10^7$, $n = 0.05$, $w = 6$, $c = 0.8$, $\alpha_i = -2$ and σ^* is slowly raised from 0 to 10^3

tent theory for comminution processes in granular materials in closed systems. Extension of this or other theories to open systems where particles can advect has not yet been achieved.

4.2 Comparison with continua

To compare the stochastic lattice rules with a continuum, we consider the evolution of a large number of cells simultaneously, and find averaged properties that represent the continuum scale. We express the breakage rate, b_i , of a single grainsize fraction s_a covering sizes over a range of Δs as

$$b_i(s_a) = \frac{\sum_{j=1}^M \mathcal{H}\left(\sigma^* - \left(\frac{s_{i,j}}{s_M}\right)^{-3/w} e^{\frac{\log(s_{i,j}/\bar{s}_{i,j})^2}{2n^2}}\right) \mathcal{H}\left(\frac{\Delta s}{2} - |s_{i,j} - s_a|\right)}{M \phi_i(s_a) \Delta t} \tag{17}$$

To solve this system globally, we need to sum over j , which represents local information about the nearest neighbours. Currently, we do not have a method for representing this information directly in a continuum model, as we inherently require information below the continuum scale, and so a new length scale must be introduced. In the stochastic lattice, the length scale which controls this behaviour is that over which the average size is computed, which for all of the simulations shown here is set to $2\Delta m$, see Eq. 4.

4.3 Cycles of crushing: towards open systems

We can extend this simulation to a quasi-open system by considering a rearrangement of particles within the stochastic lattice model, but without true advection.

After the system has reached steady state, and no further crushing will occur, we shuffle the system, relocating all

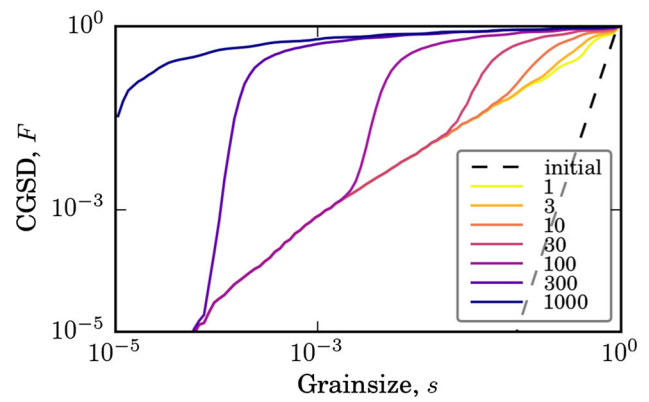


Fig. 9 Cycles of breakage towards an attractor. *Top* cumulative grainsize distributions at different numbers of cycles of loading. Each line represents the grading after a number of crushing-remixing cycles. The initial grainsize distribution is a power law with slope $\alpha = -2$. After one iteration, the system reaches $\alpha = 2$. After many successive iterations, the system approaches $\alpha = 3$

of the nearest neighbours, and resume crushing until a new steady state is reached. We can continue this cycle until an *ultimate* steady state is reached.

We begin with the simulation shown in the top left of Fig. 6, which has an initial grading defined by $\alpha_i = -2$, and after one full crushing iteration process has reached $\alpha = 2$. After crushing, the values in each cell of the simulation are randomly shuffled. This is equivalent to experimentally removing the sample from whatever loading device has crushed the sample, stirring the fragments, and then placing them back inside the device. At this stage, the sample is reloaded, which in the case of the stochastic lattice model means again increasing σ^* along the same loading path. This process is repeated many times. As progressively more iterations occur, a region of higher slope develops at larger grainsizes, and this propagates to lower grainsizes with increasing iterations, as shown in Fig. 9. The final state has been shuffled and crushed 1000 times, tending towards an ultimate grading with a new power law gradient of $\alpha = 3$.

This effect of cycles of crushing towards $\alpha = 3$ has been observed experimentally [41], numerically with a crushable discrete element method [42] and predicted analytically as the maximum entropy path towards the least efficient packing of the system [40]. It is remarkable that such a simple system as this can replicate the statistical properties of the packing involved in such a complex system.

5 Open systems

In order to model open systems, where particles can advect between points in space, we need rules for advection. To be a physically representative model, we must satisfy the conservation equation for grainsize ϕ , as shown in Eq. 2.

We set up our rules for the stochastic lattice model such that this conservation law is held for some applied velocity \mathbf{u} . The first mechanism we consider is due to segregation. Towards this end, we begin with the simplest case of segregation and describe bimixtures, where we present a model similar to that proposed in [43].

5.1 The segregation mechanism

As particles flow they collide, creating new void spaces which are preferentially filled by smaller particles, as indicated schematically in Fig. 10. The rate of creation of void spaces is governed by the shear strain rate, $\dot{\gamma}$ [2].

The simplest description of this system in terms of grain-size is shown on the left of Fig. 11 for a bimixture of sizes s_m and s_M , where the swapping frequency f is defined such that small particles always move down, and large particles move up. This representation of the was extended to describe polydisperse materials by using the formulation developed in [7,20], where it was shown through energy considerations that if a particle is larger than the local average, it has some probability of moving up, and conversely if it is smaller than the average it will move down. Increasing distance in the s direction from the average will increase the likelihood of swapping linearly. This is shown on the right of Fig. 11.

We facilitate this movement by swapping the grainsize at location $s_{i,j}$ with that either above, at $s_{i+1,j}$, or below, at

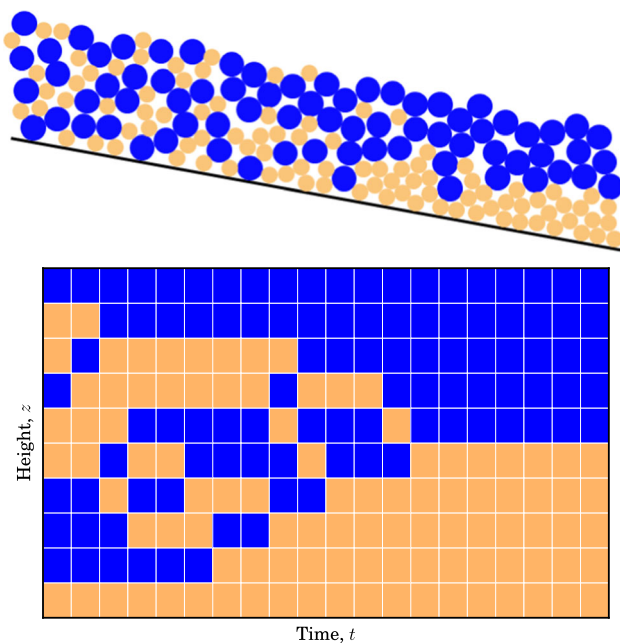


Fig. 10 Bidisperse stochastic lattice. *Top* schematic representing bidisperse segregation in 2D flow down an inclined plane. *Bottom* the complimentary 1D stochastic lattice, where large particles and small particles swap over time

$s_{i-1,j}$, depending on whether it is larger or smaller than the average size $\bar{s}_{i,j}$, as defined in Eq. 4. We define the rate of swapping as

$$f = k_s |\dot{\gamma}_i| (s_{i,j} / \bar{s}_{i,j} - 1), \tag{18}$$

where k_s is a positive non-dimensional parameter controlling the rate of segregation, and the direction of segregation is set by the sign of f . The advection of grainsize is then implemented as

$$\begin{aligned} s_{i,j}(t + \Delta t) &= s_{i+\text{sgn}(f),j}(t) \\ s_{i+\text{sgn}(f),j}(t + \Delta t) &= s_{i,j}(t), \end{aligned} \tag{19}$$

where sgn is the signum operator. We iterate in two half time steps, alternately applying this rule firstly to all odd rows, and then all even rows, so that particles are inhibited from moving very large distances in a single time step. Additionally, we only allow swapping upwards if the particle is larger than the one above it, or smaller than the one below it if moving downwards.

5.2 Bidisperse segregation

To model a simple bidisperse material, we take a single column of a bimixture ($M = 1$), of equal proportions of sizes s_m and s_M , randomly allocated to cells, and allow it to segregate under simple shear with $\dot{\gamma}(z) = 1$ and $k_s = 1$. The result is shown in the top left of Fig. 12. We can then run the simulation with $M = 10$ and average in the m -direction. The result of this is shown in the top right of Fig. 12. We can do this repeatedly, to get an increasingly resolved image of the process, as shown in the bottom row of Fig. 12 for $M = 100$ and 1000. With increasing resolution, this converges on the analytic solution presented in [7] and [3].

Figure 13 shows the average grainsize at each height over time for two different shear regimes, each for 3 different initial concentrations of small particles, s_m . The top row depicts simple shear, as in Fig. 12, while the bottom row uses a simplified version of the shear strain rate profile predicted in [7] for the case of inclined plane flow: $\dot{\gamma} = \sqrt{(1-z)}/\bar{s}$. In each case, complete segregation is observed, where every large particle lies above every small particle. The non-uniform shear strain rate in the bottom case causes non-uniform transient behaviour towards a steady grading that is the same as the top case.

As shown in [43], this model represents a simple analogy of the analytic works done by [2,3] to model bidisperse segregation, with a simple extension to multicomponent and polydisperse systems, as introduced in [20,44], and shown below.

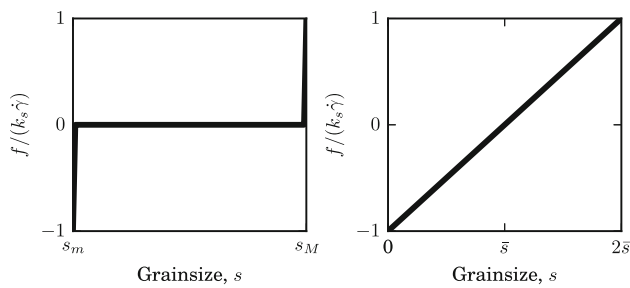


Fig. 11 Comparison of proposed segregation mechanisms as a function of grainsize s . *Left* bidisperse rule used previously in [43] *Right* polydisperse rule used in [20], where segregation frequency is a function of distance to the local mean size

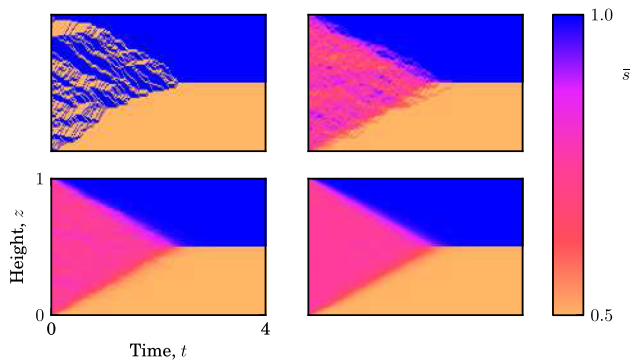


Fig. 12 Time evolution of the average grainsize \bar{s} of a bidisperse simulation with varying M subject to segregation only. All cases have $k_s = 1$ and $N_x = 100$. *Clockwise from Top left* $N_m = 1, 10, 100$ and 1000 . For the case of $N_m = 1$ we calculate the local average grainsize in the z -direction, rather than the m -direction. *Bottom right* Black lines indicate positions of concentration shocks from solution of the equivalent continuum equation

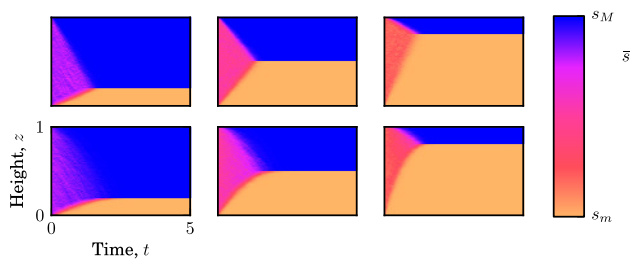


Fig. 13 Time evolution for bidisperse shear flows subject to segregation. For all cases $k_s = 1$. *Left to right* the system is initially filled with 20, 50 and 80% small particles respectively. *Top row* simple shear, where $\dot{\gamma} = 1$. *Bottom row* inclined plane flow shear condition, where $\dot{\gamma} = \sqrt{1-z}$

5.3 Polydisperse segregation

We can create a polydisperse sample by generating initial conditions in the same way as previously described for the breakage stochastic lattice model, using Eq. 16. The segre-

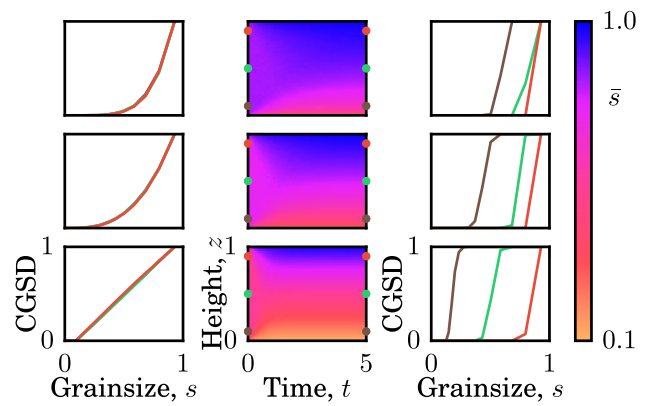


Fig. 14 Time evolution for polydisperse segregation under simple shear. For all cases $k_s = 1$ and $\dot{\gamma} = 1$. *Top to bottom* each row represents a single simulation with initial condition defined by $\alpha_i = -2, 0$ and 2 respectively. *Left* initial cumulative grainsize distribution at three different heights. The *solid red, green and brown lines* represents $z = 0.9, 0.5$ and 0.1 respectively, as indicated on the middle plot. *Middle* plot of the average grainsize \bar{s} over height and time. *Right* final grainsize distributions, plotted in the same manner as the initial cumulative grainsize distributions (colour figure online)

gation patterns produced for a range of initial conditions at constant segregation rate $k_s = 1$ and with $\dot{\gamma} = 1$ are shown in Fig. 14. Since this is now a polydisperse sample, we can calculate the grainsize distribution $\phi(s)$. On the left hand side of Fig. 14 are initial cumulative grainsize distributions, which are homogeneous in the z -direction. During the simulation, segregation occurs, creating a heterogeneous steady state condition after some time. These grainsize distributions, which now vary with height, are shown on the right hand side of the same figure.

Averaging over all M cells at a given height i , we can express the mean segregative velocity u_i of a single grainsize fraction centred at s_a from all cells at height i in a time Δt as

$$u_i(s_a) = \frac{1}{M} \sum_{j=1}^M f_{i,j}(s_a) = \frac{k_s |\dot{\gamma}_i|}{M} \sum_{j=1}^M \left(\frac{s_a}{\bar{s}_{i,j}} - 1 \right). \quad (20)$$

We have included the local average grainsize $\bar{s}_{i,j}$ in the formulation so that we know which particles are locally small or large. As particles are being swapped between heights—between representative volume elements at the continuum scale—we only require a single average grainsize per height, and can in this case freely extend the neighbourhood domain over which we find the average grainsize \bar{s} to include every cell at height j , labelling it now $\bar{s}_i = 1/M \sum_{j=1}^M s_{i,j}$. In this case, the mean velocity can be expressed as

$$u_i(s_a) = k_s |\dot{\gamma}_i| \left(\frac{s_a}{\bar{s}_i} - 1 \right). \quad (21)$$

Compare this with the analytic description of the segregation velocity with no diffusion as predicted by [7] for a continuum with internal grainsize coordinate s ,

$$u(s) = |\dot{\gamma}| \frac{g \cos \theta}{c} \left(\frac{s}{\bar{s}} - 1 \right), \tag{22}$$

where c is a fitting parameter, g is the acceleration due to gravity, and θ is the angle of the plane down which flow is occurring. As shown in [45], lattice models can successfully be used as a coarse finite differencing method to describe systems such as these without resorting to flux limited finite volume schemes, as would otherwise be necessary [46,47].

This stochastic lattice model, together with the rule for remixing, which will be shown next, represents the simplest description of the analytic model presented in [7].

5.4 Remixing

In nature we rarely see such perfect segregation as that pictured above. This is due to the random fluctuation of particles as the flow propagates down slope. As has been done before analytically [46], we can capture this effect by introducing remixing into the flow. For the simplest case, we allow particles to swap randomly either up or down with some frequency, given by a constant $D/\Delta z^2$. At this stage we let this probability be independent of the shear strain rate $\dot{\gamma}$, although a strong dependency has been observed [48] in experiments. With frequency of swapping controlled by the diffusivity, D , swapping is implemented by drawing a discrete i.i.d. random variable, Y , from the two integer values $\{-1, 1\}$, and using

$$\begin{aligned} s_{i,j}(t + \Delta t) &= s_{i+Y,j}(t) \\ s_{i+Y,j}(t + \Delta t) &= s_{i,j}(t). \end{aligned} \tag{23}$$

An example of the mixing rule acting on a single column of cells over time is shown in Fig. 15. Initially, the system is perfectly segregated, but over time the systems becomes randomised due to the presence of mixing. The characteristic time for mixing to occur is the inverse of the diffusivity D/H^2 , where $H = N_x \Delta x$.

We are effectively describing a system of cells undergoing Brownian motion, whereby particles move by the application of random forces over time scales that are short relative to the motion of the particle. When considered over long time scales and large numbers of particles, this is analogous to Fickian diffusion [48]. This is one of a large set of cellular automata that exist to model pure diffusion [49].

As in the case of segregation, this process can be averaged over the m -direction to describe the evolution of the average grainsize at any height over time. By increasing M , we can increase the smoothness of our solution. Figure 16

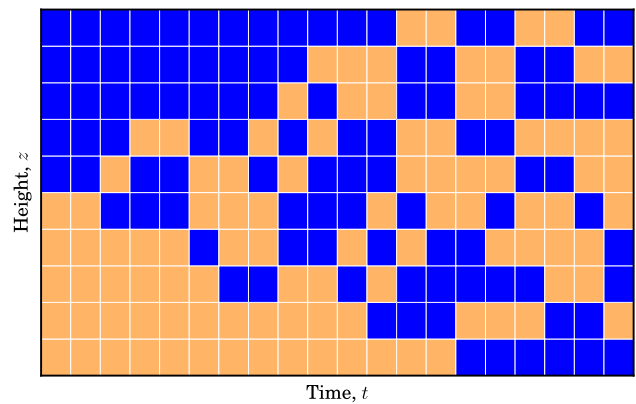


Fig. 15 An illustration of the mixing mechanism. Ten cells, initially segregated with all large particles (blue) above small particles (yellow), subjected to the mixing mechanism only. Over time, the system reaches a disordered state (colour figure online)

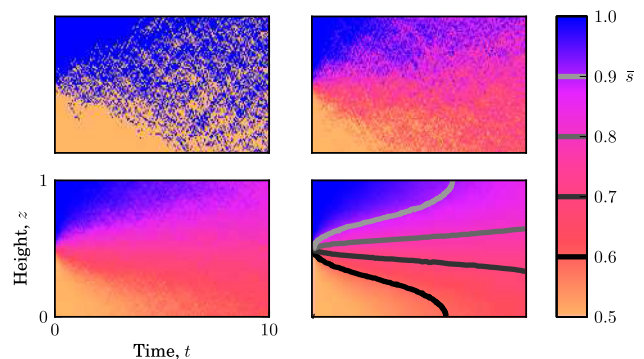


Fig. 16 Time evolution of the average grainsize \bar{s} of a bidisperse simulation with varying N_m subject to mixing only. All cases have $D = 0.01$ and $N_x = 100$. Clockwise from top left $N_m = 1, 10, 100$ and 1000 . Bottom right solid lines indicate contours from solution of the equivalent continuum equation

shows the same system as Fig. 15, initially segregated, that mixes over time to create a homogeneous system, but now for increasing M . This diffusive behaviour can be described at the continuous limit using Fick’s first law of diffusion,

$$\frac{\partial \phi}{\partial t} = D \frac{\partial^2 \phi}{\partial z^2}. \tag{24}$$

6 Coupled problems

We now have three distinct processes which can be described simultaneously in a single simulation. These have all been shown above with their analogous continuum description, yet not in all cases could a direct link be shown. For the case of comminution, an internal length scale governing the spatial distribution of grainsize over a sub-continuum length scale was required.

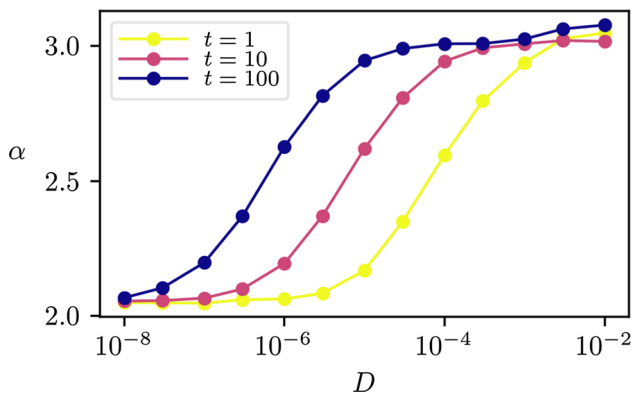


Fig. 17 Coupled comminution and mixing. For all cases, $\sigma^* = 10^3$, $n = 0.05$, $c = 0.8$, $w = 6$, $N_x = 100$ and $N_m = 1000$. Plot shows value of the best fit to the power law part of cumulative grainsize distribution at $t = 1, 10$ and 100 . Over time, the system moves from the initial grading ($\alpha = -2$) towards a final value of $\alpha \approx 3$

As all of the mechanisms previously described have been created in the same framework, we can simply run a stochastic lattice model which includes multiple phenomena at the same time. As will be shown in this Section, we can investigate the interactions between the mechanisms by varying the parameters which control their effects.

6.1 Comminution and mixing

We begin with a stochastic lattice model that includes both comminution and mixing. This system represents an extension of the cycles of crushing pictured in Fig. 9, but now with true advection. In this case, as in Fig. 9, we expect that after a short time relative to the diffusive time, the system will reach $\alpha_f = 2$, as significant mixing has not yet occurred. At longer times, the system will approach $\alpha_f = 3$, and its final grading. This effect was explored in [20], and here is captured in Fig. 17, where the diffusive time is controlled by the ratio D/H^2 .

For vanishingly small diffusivities, the system will still approach $\alpha_f = 3$, but only after very long periods of comminution. Conversely, at very large diffusivities, the system passes $\alpha_f = 2$ very rapidly, and approaches $\alpha_f = 3$ in a relatively short time.

6.2 Segregation and mixing

In flows of polydisperse granular materials where comminution does not occur, we can model the evolution of the grainsize distribution as being comprised of segregative and diffusive remixing components. This occurs in many industrial mixing processes, and well describes levee formation and runout characteristics in landslides [50,51]. At higher speeds remixing increases, suppressing segregation, while at

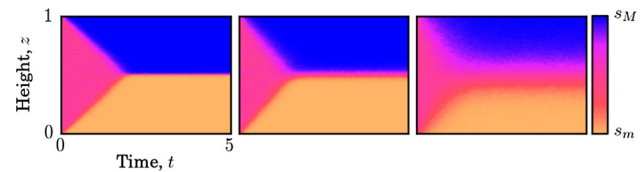


Fig. 18 Bidisperse segregation under simple shear with diffusion. Left to right increasing diffusivity $D = 0.002, 0.01$ and 0.05 with constant segregation coefficient $k_s = 1$. Increasing the mixing coefficient smooths out concentration shocks in the spatial direction, giving more physically realistic solutions

low speeds segregation can play a dominant role in the flow behaviour.

The effect of coupling mixing and segregation in a bimixture can be seen in Fig. 18, where increasing diffusivity D smooths out the concentration shock between the two phases of large and small particles. This can be treated in an identical manner for polydisperse mixtures. This has been shown analytically for bidisperse systems in [46] and validated experimentally in [52].

Generally, solving these systems of equations numerically requires the suppression of spurious numerical diffusion with sophisticated finite differencing schemes [47]. This behaviour stems from the non-linearity of the underlying equations, but is not an issue for numerical solutions obtained using stochastic lattice models [45].

6.3 Segregation and comminution

In many situations, segregation and comminution occur simultaneously in a flow situation, such as in the grain milling depicted in Fig. 2. In other cases, it is not even clear if segregation has occurred, yet particles are advecting in space and strong comminution is observed, such as in earthquake faulting and snow avalanches. In many of these cases, we observe log-normal grainsize distributions, rather than power law distributions, which exist at all depths of flow. Unlike power law grainsize distributions, log-normal distributions contain a characteristic size directly related to their mean value. As a result, the existence of depth-dependent mean values of log-normal grainsize distributions in crushable polydisperse granular flows in nature is reminiscent of unconstrained size-dependent segregation competing with size-independent comminution. A log-normal distribution is one that obeys the following scaling for the cumulative grainsize distribution F_{LN} ,

$$F_{LN} = \frac{1}{2} \operatorname{erfc} \left(-\frac{\log s - \mu}{\sigma \sqrt{2}} \right), \quad (25)$$

where μ and σ are location and scale parameters, and erfc is the complimentary error function.

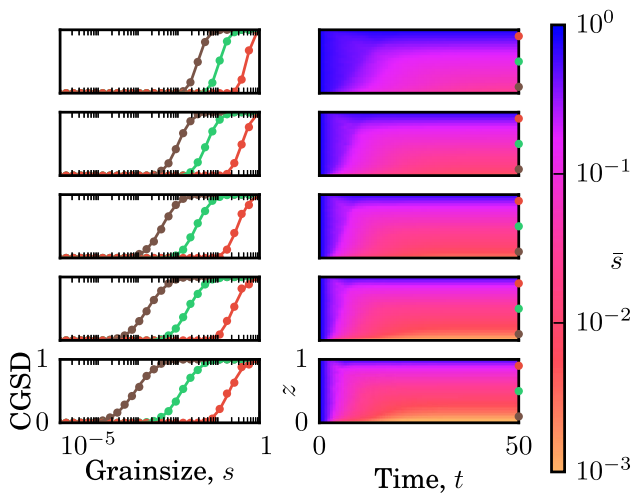


Fig. 19 A crushable flow with two mechanisms: segregation and comminution. Initially, the system is homogeneous, being a polydisperse sample with initial grainsize distribution defined by $\alpha_i = -2$. *Top to bottom* three cases are considered with varying $D = 10^{-4}, 10^{-2}$ and 10^0 . *Right* spatiotemporal evolution of the average grainsize. *Left* cumulative grainsize distribution at three points in the flow, corresponding to the *circles* in on the *right*. *Lines* are best fit lognormal distributions

In the results shown in Fig. 19, both segregation and comminution mechanisms are present. For all cases, log-normal cumulative grainsize distributions are observed over all depths. When tested against a null hypothesis, the assumption that the data is log-normally distributed gives p-values from the bottom half of generally <0.001 , as measured using a normalcy test [53].

As expected, increasing the applied stress, σ^* , increases the level of particle crushing, producing progressively smaller fragments. The time to reach a steady state in terms of the average grainsize, \bar{s} , however is approximately constant. It is evident that significant changes in the grainsize distribution will not occur indefinitely, and some steady state is reached in a finite time.

6.4 Segregation, mixing and crushing

As shown previously in [20], we can now couple all three mechanisms and observe the evolution of the grainsize distribution as all of the constituent mechanisms interact. Each time step, we first check each cell and if the breakage rule is met, we change the cell’s grainsize. Secondly, we iterate over all of the cells and swap them with a neighbour if the segregation rule is met. Finally, we again iterate over all cells and if the diffusion rule is met, we swap randomly with a neighbour.

We now have a system that models avalanche and landslide flow, where particles at the base are sheared and crush, creating a layer which may enhance flow, such as in Fig. 19. The inclusion of mixing in the system, as shown in Fig. 20,

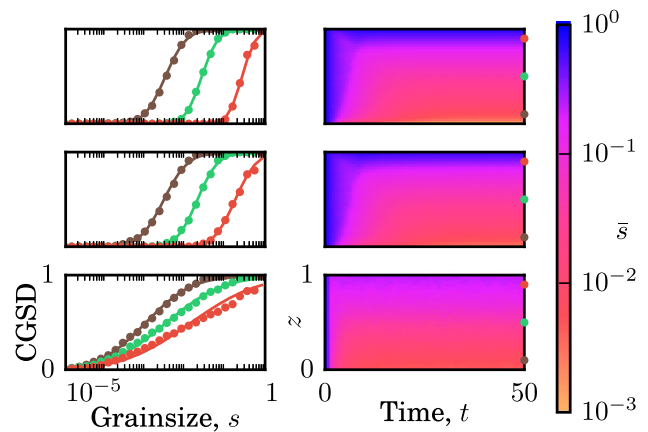


Fig. 20 A crushable flow with all three mechanisms. Initially, the system is homogeneous, being a polydisperse sample with initial grainsize distribution defined by $\alpha_i = -2$. *Top to bottom* three cases are considered with varying $D = 10^{-4}, 10^{-2}$ and 10^0 . *Right* spatiotemporal evolution of the average grainsize. *Left* cumulative grainsize distribution at three points in the flow, corresponding to the *circles* in on the *right*. *Lines* are best fit lognormal distributions

enhances the spread of sizes produced by comminution. Again, log-normal cumulative grainsize distributions are measured, which represent those found in many geophysical processes, such as in snow avalanches [54], pyroclastic flows [55,56], debris flows [57,58], and rock avalanches [59].

6.5 An equivalent continuum model

Considering conservation of mass alone, we can express all three mechanisms in a heterarchical continuum form as

$$\frac{\partial \phi}{\partial t} + k_s \frac{\partial}{\partial z} \left(\phi |\dot{\gamma}| \left(\frac{s}{\bar{s}} - 1 \right) \right) = D \frac{\partial^2 \phi}{\partial z^2} + b\phi - \int_s^{SM} P(s|s')b(s')\phi(s') ds'. \tag{26}$$

This population balance model differs from the stochastic lattice model in the sense that the internal coordinate s does not retain information about local neighbours that is present when using m . Because of this, we cannot at this stage describe the comminution process concurrently with segregation and mixing in a continuum form. This omission gives an important insight into the use of continuum theories to represent internally (i.e. within the representative volume element) spatially correlated material.

For the mechanisms of segregation and mixing, the length scale representing the local neighbourhood is not an important consideration. However for comminution, it must be included as part of the model to enable us to predict the correct final distribution.

7 Conclusions

We have developed the paradigm of a heterarchical multiscale model, in this instance formulated as a stochastic lattice, that can successfully capture microscale continuum properties at the macroscale. Two alternative formulations of the internal coordinate choice at the microscale were discussed, and it was shown that describing just the grainsize distribution allows us to successfully model segregation and mixing, but the addition of information about the local particle arrangement allows for the modelling of comminution. While work is still needed to bridge the gap between the two proposed internal coordinates analytically, there is promise that in the near future these mechanisms can be described purely as continuum properties, and that these ideas could inform new, micro-inspired constitutive frameworks.

The stochastic lattice developed here was shown to reproduce the behaviour of segregation, mixing and comminution, both in isolation and in combination. By assembling all three stochastic lattice models together we were able to explore the interactions between these phenomena. One outcome is that in closed systems, crushable granular material are limited by power laws, however during flow the interaction with segregation causes the system to be limited by log-normal distributions.

The success of this stochastic lattice model is that it enables us to study the evolution and limits of the grain-size distribution in a variety of scenarios. In the future, we envisage that heterarchical models can be used to represent a wide variety of multiscale phenomena.

Acknowledgements The authors would like to thank Prof Ken Kamrin for insightful discussions regarding the nature of the microstructural coordinate. IE acknowledges support from the ARC through DP130101291 and DP160104310 grants.

Compliance with ethical standards

Conflict of interest The authors declare that they have no conflict of interest.

References

- Jop, P., Forterre, Y., Pouliquen, O.: A constitutive law for dense granular flows. *Nature* **441**(7094), 727 (2006)
- Savage, S., Lun, C.: Particle size segregation in inclined chute flow of dry cohesionless granular solids. *J. Fluid Mech.* **189**, 311 (1988)
- Gray, J.M.N.T., Thornton, A.: A theory for particle size segregation in shallow granular free-surface flows. *Proc. R. Soc. A* **461**(2057), 1447 (2005)
- Magloughlin, J.F., Spray, J.G.: Frictional melting processes and products in geological materials: introduction and discussion. *Tectonophysics* **204**(3–4), 197 (1992)
- Gan, Y., Rognon, P., Einav, I.: Phase transitions and cyclic pseudotachylite formation in simulated faults. *Philos. Mag.* **92**(28–30), 3405 (2012)
- Einav, I.: Breakage mechanics—part 1: theory. *J. Mech. Phys. Solids* **55**(6), 1274 (2007)
- Marks, B., Rognon, P., Einav, I.: Grainsize dynamics of polydisperse granular segregation down inclined planes. *J. Fluid Mech.* **690**, 499 (2012)
- Cowin, S.C., Satake, M.: Continuum mechanical and statistical approaches in the mechanics of granular materials. *J. Rheol.* **23**(2), 243 (1979)
- Goldhirsch, I.: Stress, stress asymmetry and couple stress: from discrete particles to continuous fields. *Granul. Matter* **12**(3), 239 (2010)
- Weinhart, T., Thornton, A.R., Luding, S., Bokhove, O.: From discrete particles to continuum fields near a boundary. *Granul. Matter* **14**(2), 289 (2012)
- Nguyen, G.D., Einav, I.: The energetics of cataclasis based on breakage mechanics. *Pure Appl. Geophys.* **166**(10), 1693 (2009). doi:10.1007/s00024-009-0518-x
- Russell, A.R., Einav, I.: Energy dissipation from particulate systems undergoing a single particle crushing event. *Granul. Matter* **15**(3), 299 (2013)
- Andrade, J.E., Tu, X.: Multiscale framework for behavior prediction in granular media. *Mech. Mater.* **41**(6), 652 (2009)
- Nitka, M., Combe, G., Dascalu, C., Desrues, J.: Two-scale modeling of granular materials: a DEM–FEM approach. *Granul. Matter* **13**(3), 277 (2011)
- Legros, F.: The mobility of long-runout landslides. *Eng. Geol.* **63**, 301 (2002)
- Imre, B., Laue, J., Springman, S.: Fractal fragmentation of rocks within sturzstroms: insight derived from physical experiments within the ETH geotechnical drum centrifuge. *Granul. Matter* **12**(3), 267 (2010)
- Iverson, R.M.: The debris-flow rheology myth. *Debris-flow Hazards Mitig. Mech. Predict. Assess* **1**, 303 (2003)
- Redner, S.: Fragmentation. Statistical models for the fracture of disordered media, New York: North-Holland **321**, 348 (1990)
- Ramkrishna, D.: Population Balances: Theory and Applications to Particulate Systems in Engineering. Academic Press, San Diego (2000)
- Marks, B., Einav, I.: A mixture of crushing and segregation: the complexity of grainsize in natural granular flows. *Geophys. Res. Lett.* **42**(2), 274 (2015)
- Toffoli, T.: Cellular automata as an alternative to (rather than an approximation of) differential equations in modeling physics. *Phys. D: Nonlinear Phenom.* **10**(1–2), 117 (1984)
- Rafler, S.: Generalization of Conway’s “Game of Life” to a continuous domain—SmoothLife ArXiv e-prints (2011)
- Randolph, A., Ranjan, R.: Effect of a material-flow model in prediction of particle-size distributions in open-and closed-circuit mills. *Int. J. Miner. Process.* **4**(2), 99 (1977)
- Peterson, T., Scotto, M., Sarofim, A.: Comparison of comminution data with analytical solutions of the fragmentation equation. *Powder Technol.* **45**(1), 87 (1985)
- McGrady, E.D., Ziff, R.M.: “Shattering” transition in fragmentation. *Phys. Rev. Lett.* **58**, 892 (1987)
- Williams, M.: An exact solution of the fragmentation equation. *Aerosol Sci. Technol.* **12**(3), 538 (1990)
- Turcotte, D.: Fractals and fragmentation. *J. Geophys. Res.* **91**(B2), 1921 (1986)
- Cheong, Y., Reynolds, G., Salman, A., Hounslow, M.: Modelling fragment size distribution using two-parameter Weibull equation. *Int. J. Miner. Process.* **74**, S227 (2004)
- Reynolds, G., Fu, J., Cheong, Y., Hounslow, M., Salman, A.: Breakage in granulation: a review. *Chem. Eng. Sci.* **60**(14), 3969 (2005)
- Steady, S., Sammis, C.: An automaton for fractal patterns of fragmentation. *Nature* **353**(6341), 250 (1991)

31. McDowell, G., Bolton, M., Robertson, D.: The fractal crushing of granular materials. *J. Mech. Phys. Solids* **44**(12), 2079 (1996)
32. Ben-Nun, O., Einav, I.: The role of self-organization during confined comminution of granular materials. *Philos. Trans. R. Soc. Lond. A Math. Phys. Eng. Sci.* **368**(1910), 231 (2010)
33. Shaebani, M.R., Madadi, M., Luding, S., Wolf, D.E.: Influence of polydispersity on micromechanics of granular materials. *Phys. Rev. E* **85**(1), 011301 (2012)
34. Cunningham, C.: The Kuz–Ram model for prediction of fragmentation from blasting. In: *Proceedings of the first international symposium on rock fragmentation by blasting, Lulea, Sweden*, vol. 2, pp. 439–53. (1983)
35. Ouchterlony, F.: The Swebrec function: linking fragmentation by blasting and crushing. *Min. Technol.* **114**(1), 29 (2005)
36. Ben-Nun, O., Einav, I., Tordesillas, A.: Force attractor in confined comminution of granular materials. *Phys. Rev. Lett.* **104**(10), 108001 (2010)
37. Ben-Zion, Y., Sammis, C.G.: Characterization of fault zones. *Pure Appl. Geophys.* **160**, 677 (2003)
38. Crosta, G.B., Frattini, P., Fusi, N.: Fragmentation in the Val Pola rock avalanche, Italian Alps. *J. Geophys. Res. Earth Surf.* **112**(F1), F01006 (2007)
39. Sammis, C., King, G.: Mechanical origin of power law scaling in fault zone rock. *Geophys. Res. Lett.* **34**(4), L04312 (2007)
40. Delaney, G., Hutzler, S., Aste, T.: Relation between grain shape and fractal properties in random Apollonian packing with grain rotation. *Phys. Rev. Lett.* **101**(12), 120602 (2008)
41. Lőrincz, J., Imre, E., Gálos, M., Trang, Q., Rajkai, K., Fityus, S., Telekes, G.: Grading entropy variation due to soil crushing. *Int. J. Geomech.* **5**(4), 311 (2005)
42. Ben-Nun, O.: Confined comminution of granular materials: self-organisation, attractors and patterns. Ph.D. thesis, University of Sydney (2010)
43. Marks, B., Einav, I.: A cellular automaton for segregation during granular avalanches. *Granul. Matter* **13**, 211 (2011)
44. Gray, J.M.N.T., Ancey, C.: Multi-component particle-size segregation in shallow granular avalanches. *J. Fluid Mech.* **678**, 535 (2011)
45. Marks, B., Einav, I., Rognon, P.: Polydisperse segregation down inclines: towards degradation models of granular avalanches. In: Bonelli, V., Dascalu, C., Nicot, E. (eds.) *Advances in Bifurcation and Degradation in Geomaterials*. Springer Series in Geomechanics and Geoengineering, vol. 11, pp. 145–151. Springer, Netherlands (2011)
46. Gray, J.M.N.T., Chugunov, V.A.: Particle-size segregation and diffusive remixing in shallow granular avalanches. *J. Fluid Mech.* **569**, 365 (2006)
47. Kurganov, A., Tadmor, E.: New high-resolution central schemes for nonlinear conservation laws and convection–diffusion equations. *J. Comput. Phys.* **160**(1), 241 (2000)
48. Utter, B., Behringer, R.P.: Self-diffusion in dense granular shear flows. *Phys. Rev. E* **69**(3), 031308 (2004)
49. Chopard, B., Droz, M.: Cellular automata model for the diffusion equation. *J. Stat. Phys.* **64**(3–4), 859 (1991)
50. Johnson, C., Kokelaar, B., Iverson, R., Logan, M., LaHusen, R., Gray, J.M.N.T.: Grain-size segregation and levee formation in geophysical mass flows. *J. Geophys. Res. Earth Surf.* **117**(F1), F01032 (2012)
51. Baker, J., Johnson, C., Gray, J.: Segregation-induced finger formation in granular free-surface flows. *J. Fluid Mech.* **809**, 168 (2016)
52. Wiederseiner, S., Andreini, N., Épely-Chauvin, G., Moser, G., Monnereau, M., Gray, J.M.N.T., Ancey, C.: Experimental investigation into segregating granular flows down chutes. *Phys. Fluids* **23**(1), 013301 (2011)
53. d’Agostino, R.B.: An omnibus test of normality for moderate and large size samples. *Biometrika* **58**(2), 341 (1971)
54. Bartelt, P., McArdell, B.W.: Granulometric investigations of snow avalanches. *J. Glaciol.* **55**(193), 829 (2009)
55. Wilson, C.: The taupo eruption, New Zealand II. The taupo ignimbrite. *Philos. Trans. R. Soc. Lond. A Math. Phys. Eng. Sci.* **314**(1529), 229 (1985)
56. Esposito, L., Esposito, A.W., Pasculli, A., Sciarra, N.: Particular features of the physical and mechanical characteristics of certain Phlegraean pyroclastic soils. *Catena* **104**, 186 (2013)
57. Schmincke, H.U.: Graded lahars in the type sections of the Ellensburg Formation, south-central Washington. *J. Sediment. Res.* **37**(2), 438–448 (1967)
58. Phillips, C.J., Davies, T.R.: Determining rheological parameters of debris flow material. *Geomorphology* **4**(2), 101 (1991)
59. Dufresne, A., Bösmeier, A., Prager, C.: Sedimentology of rock avalanche deposits—case study and review. *Earth Sci. Rev.* **163**, 234 (2016)